JCSE The Journal of Corrosion Science and Engineering

21st Century Corrosion Science

CORROSION BEHAVIOR OF LASER SURFACE MELTED 2014 ALUMINIUM ALLOY IN T6 AND T451 TEMPERS

P.H. Chong*, Z. Liu, P. Skeldon and G. E. Thompson

Corrosion and Protection Centre,
University of Manchester Institute of Science and Technology, P.O. Box 88,
Manchester M60 1QD, UK

Abstract

It is generally accepted that laser surface melting (LSM) can be used for improving the localised corrosion resistance of various metallic alloys as a result of homogenisation and refinement of microstructures, and phase transformations. However, there are exceptions. For example, no improvement of pitting corrosion resistance of a wide range of aluminium alloys by LSM has been reported. This paper investigates the corrosion performance of laser-melted Al 2014 alloy in the T6 and T451 conditions to determine the key factors influencing pitting corrosion performance. LSM was carried out using a 3 kW CW Nd:YAG laser with a line beam profile. Examination of laser-melted surfaces in terms of microstructure, elemental distribution and phase analysis was performed using SEM/EDX, EPMA and XRD. Pitting corrosion resistance was evaluated using potentiodynamic anodic polarisation in de-aerated 1 M NaCl solution. Laser treatment enhanced the pitting potential by up to 170 and 110 mV for the T6 and T451 conditions respectively. The major factor contributing to the improvement appeared to be alloying elements, mainly of copper, in the aluminium matrix with refinement of the microstructure, with finer intermetallic particles, appear to playing a lesser role.

Keyword: Laser surface melting; Pitting corrosion; Al 2014 alloy.

*Corresponding Author: Tel: +44 161 236 3311 (ext. 2920); Fax: +44 161 200 4865;
Email: p.chong @postgrad.umist.ac.uk

This paper was presented at the Conference "Corrosion Science in the 21st Century" held at UMIST in July 2003.

1. Introduction

Laser surface melting (LSM) offers significant potential for improving surface properties, such as corrosion and wear resistance. It is generally accepted that the improvement in corrosion performance is due to refinement/homogenisation of microstructure and dissolution/redistribution of precipitates or inclusions, which result from rapid solidification. LSM has been used to improve pitting corrosion resistance of austenitic stainless steels, with shifts of the pitting potential by up to 400 mV resulting from elimination or reduction of MnS inclusions that are believed to be common sites for initiation of pitting [1]. However, LSM may offer little benefit to the corrosion resistance of some materials, for instance, many aluminium alloys. Thus, although LSM has been reported to raise the pitting potential of Al 2014-T6 alloy [2], other work has shown no improvement in pitting corrosion resistance of 2024-T351 alloy in 3 wt% NaCl solution [3], Al-Si alloy in 10 wt% HCl and 5 wt% NaCl solutions [4], Al 3003 alloy in 0.1 M NaCl solution [5] and Al 7075 alloy in 3 wt% NaCl solution [6]. To date, no detailed explanation has been given for these contrasting behaviours, in particular concerning the relationship between microstructure and electrochemical response. Therefore, the purpose of this study is to investigate the corrosion performances of laser-melted Al 2014 alloy in the T6 (artificial ageing) and T451 (natural aging) conditions to determine the key factors influencing pitting corrosion performance.

2. Experimental procedure

AISI 2014 alloy, nominal composition (wt%) 3.9 – 5 Cu, 0.2 - 0.8 Mg, 0.4 - 1.2 Mn, 0.5 - 1.2 Si, 0.7 Fe (max), 0.1 Cr (max), and balance Al of 8 mm thickness, in the T6 and T451 tempers, was used for this study. A 3 kW CW Nd:YAG laser, with a line beam source produced by a parabolic line segmented optic, was utilized with Table 1 providing the laser operating parameters employed. Figure 1 shows the power density distribution of the laser beam along the y and x axes corresponding to the width of the laser beam and the direction of beam traverse respectively. Prior to laser treatment, the surface of each specimen was sandblasted by 99.9% Al_2O_3 ,with grit diameter 62-74 μm, to enhance the surface absorption. Argon gas was passed over the melt pool at 20 l/min to prevent surface oxidation.

After laser treatment, the characterisation of microstructure, chemical composition and phase formation was carried out by scanning electron microscopy (SEM) with associated elemental analysis by energy dispersive X-ray (EDX) spectroscopy, electron probe microanalysis (EPMA) and X-ray diffraction (XRD). The electrochemical behaviours of the as-received and the laser-treated specimens were examined in deaerated 1 M NaCl solution at 30 °C. Specimens were mounted in epoxy resin, ground and then polished to a 1 μm diamond finish. The solutions were deaerated by initial purging with nitrogen for 45 min and with continued purging throughout the test. The specimens were immersed in the solution for 50 min to stabilize the open circuit potential. Anodic polarisation curves were then determined at a potential scan rate of 0.167 mV/s using a Schlumberger SI 1280 computer-controlled potentiostat and a conventional three-electrode cell employing a platinized titanium counter electrode and a saturated calomel reference electrode (SCE).

Table 1 Laser operating parameters for surface melting of 2014 alloy at a laser power of 3 kW (A: T6 and B: T451)

Specimen No.		Beam dimension, x-y axis (mm)	Traverse speed, (m/min)
A1	B1	2 x 6	2
A2	B2		2.25
A3	B3		2.5
A4	B4		2.75
A5	B5	2 x 10	0.1
A6	B6		0.25
A7	B7		0.75

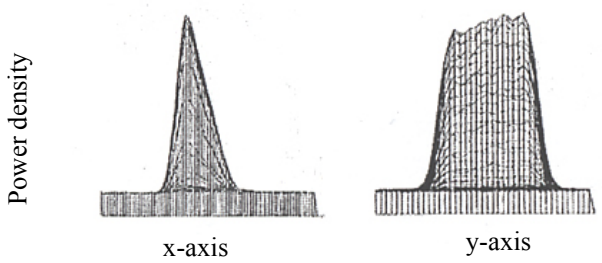

Fig.1 Power density distribution for the line beam.

3. Results and Discussion

As-received Al 2014 alloy in both the T6 and T451 conditions contained similar intermetallic particles distributed randomly in the aluminium matrix (Figure 2); SEM/EDX distinguished three types of precipitates: Type 1 – roughly spherical Al-Cu particles, of approximate size 5-15 μm, Type 2 - large, 10-20 μm, but irregular shaped Al-Cu-Mn-Fe-Si particles, and Type 3 – Mg-Si particles, of size 2 μm, adjacent to the Al-Cu particles. Types 1 and 3 are assigned to Al_2Cu and $MgSi_2$ phases, which were identified by XRD (Figure 3). These analyses agree with findings in the literature [7,8]. The alloy also revealed a preferred orientation of the matrix grows in the [111] direction.

After the laser treatment, the surfaces appeared very smooth. For a given power and beam size, the melt pool geometry changed from hemispherical to flat-bottomed with increase of traverse speed as thermal diffusion became limited. The flat-bottomed shape is desirable for most laser surface treatments. Similar solidification microstructures were found for both tempers of the alloy, consisting of columnar cells that had grown epitaxially from the unmelted substrate (Figure 4). A thin layer of planar front zone, of thickness 3-5 μm was located at the fusion boundary with the substrate. Beyond this interface, the microstructure changed rapidly from cellular to cellular dendritic/dendritic. Such microstructures were in accord with the high initial ratio of thermal gradient G and solidification rate R when solidification began, and its fall-off as solidification proceeded towards the free surface. The cellular layer was very narrow, approximately 20 μm, due to the rapid variation of the G/R ratio.

The solidification microstructure within the melted zone consisted of a continuous network of second phase precipitates, appearing as light areas at dendrite boundaries, enveloping aluminium matrix phase, of dark appearance. Microsegregation of alloying elements, mainly of copper, but also of magnesium and manganese and silicon, which occurred when the solute was rejected at the liquid/solid interface, and a boundary layer enriched in alloying elements developed in the liquid immediately ahead of the solidification front, resulting in the formation of precipitates in the interdendritic spaces. The solute segregation was highly dependent on the thermal

process in terms of thermal gradient, solidification rate and cooling rate that were determined by the laser operating conditions. Heat-transfer calculations [9] show that the cooling rate increases rapidly from the fusion boundary towards the surface. Thus, the dendritic arm spacing increased from 2 μm at the surface to 4 μm at the boundary (Figure 5). Similarly, under constant laser power and beam size, increasing traverse speed, and hence increasing cooling rate, reduced the spacing. Further, the combination of lower power density and longer interaction time for the 10 mm laser beam than those of the 6 mm beam produced a much slower cooling and hence a greater dendritic arm spacing.

Generally, microsegregation increased with decreasing cooling rate, similar to that of dendritic arm spacing. Thus, the copper concentration within the planar front zone of specimen A7 by EPMA was 1.5 wt%, and increasing to 2.5 wt% in dendritic cores, i.e. in the α-Al matrix, close to the faster cooling surface area. These values compare with an estimated 0.04 wt% Cu, the equilibrium matrix concentration, for the as-received alloy. The copper concentration within dendritic cores was also found to increase with increasing of traverse speed, i.e with increasing cooling rate, from 1.7 wt% for specimen A5 to 2.5 wt% for specimen A7. Further, EPMA mapping of specimen B1 disclosed that enrichment of copper, magnesium, manganese and silicon in dendritic boundaries, Figures 6 and 7, which became more pronounced towards the fusion boundary. Specimens treated with the 6 mm beam presented less copper segregation along the dendritic boundaries than those treated with the 10 mm beam due to the further cooling rate with the narrow beam.

The average value of the magnesium concentration in laser-treated specimens decreased to 0.3 wt%, compared with 0.8 wt% of the as-received alloy, due to the selective vaporisation of magnesium during laser melting, which was been reported previously for LSM of Al 2024 alloy [3]. EPMA mapping indicated magnesium and silicon in precipitates with a low population density. XRD disclosed θ-Al_2Cu and α-Al, with a preferred orientation of the lattice in the [200] direction that increased with decreasing cooling rate (Figures 8 a-b). Due to the resolution limitations of EDX and EPMA, it was not possible to measure the precise compositions of the various

microstructural regions, for specimens treated with the 6 mm beam, with dendritic arm spacing of 1-2 μm.

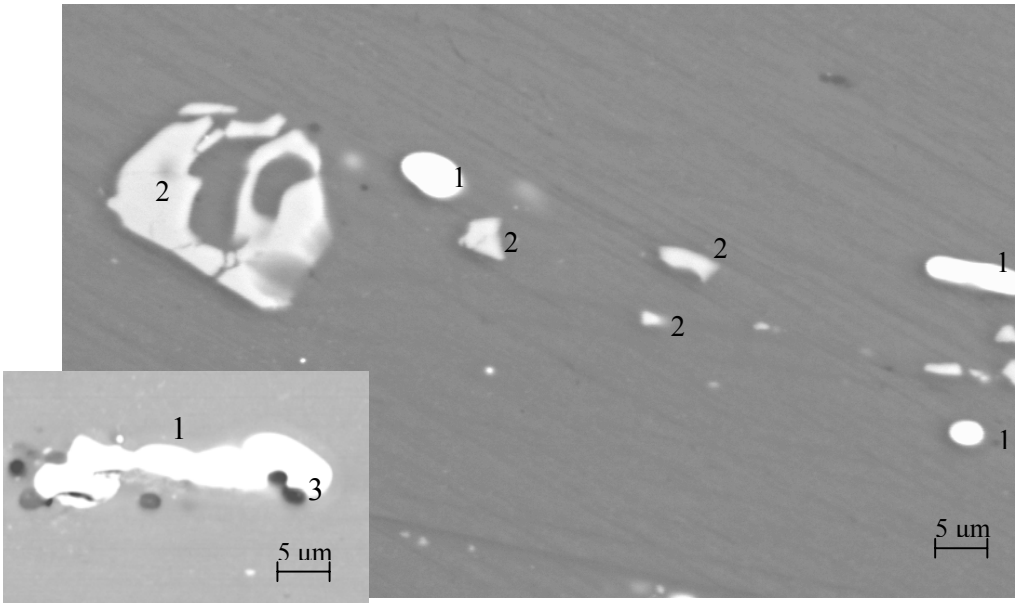

Figure 2 Second phase particles in 2014-T451 alloy. Type 1: Al_2Cu phase; Type 2: Al-Cu-Mn-Fe-Si phase; Type 3: Mg_2Si particles adjacent to Al_2Cu phase.

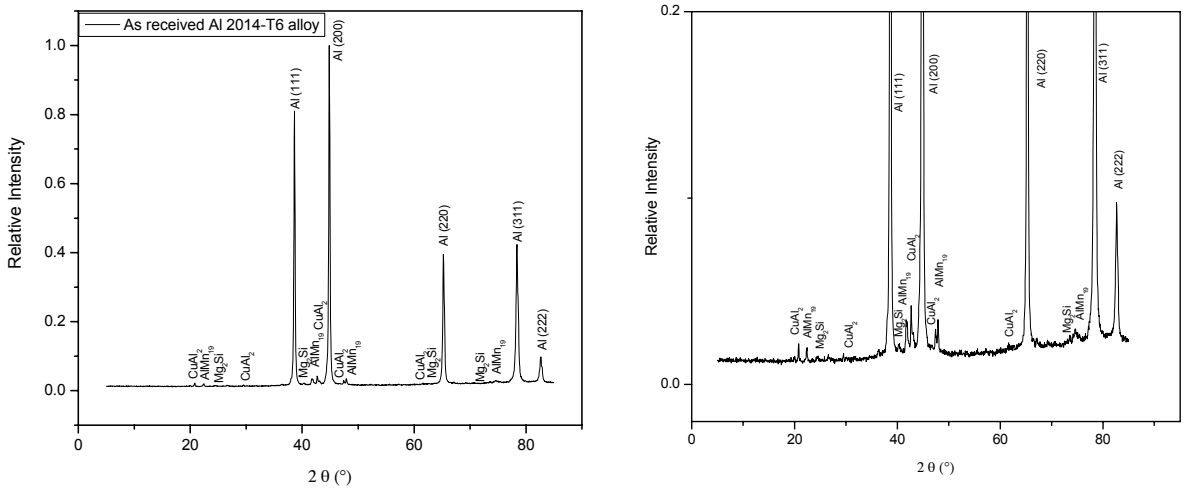

Figure 3 XRD data of 2014-T6 alloy. (a) as-received alloy; (b) as-received alloy with high magnification of the peaks .

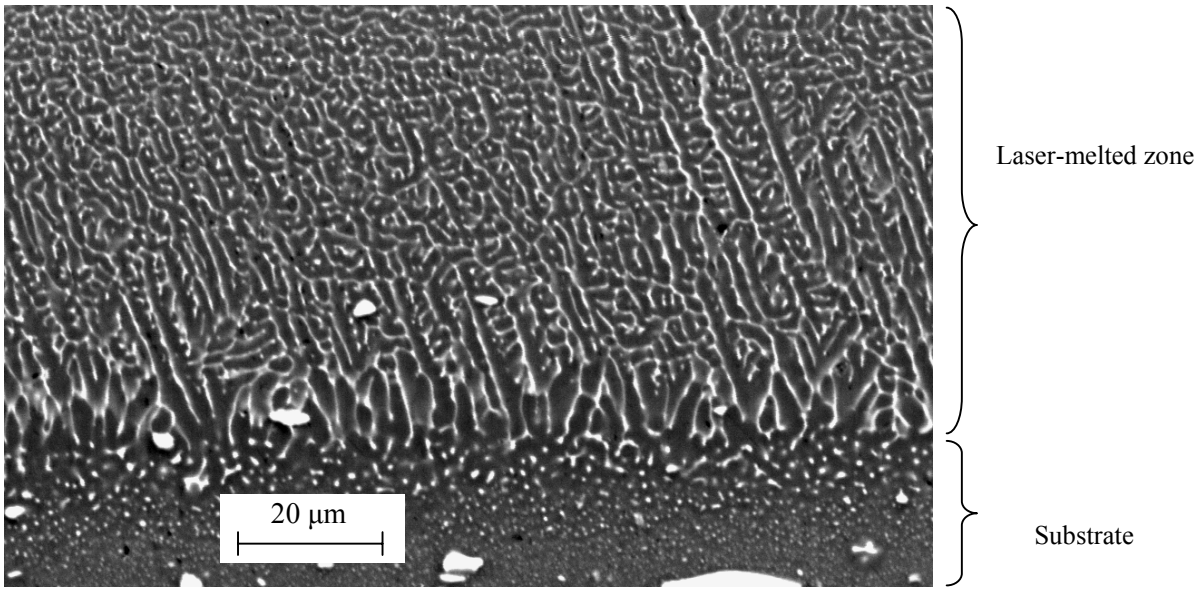

Figure 4 Scanning electron micrograph of a typical cross section of the laser-melted 2014-T451 alloy, specimen B2 .

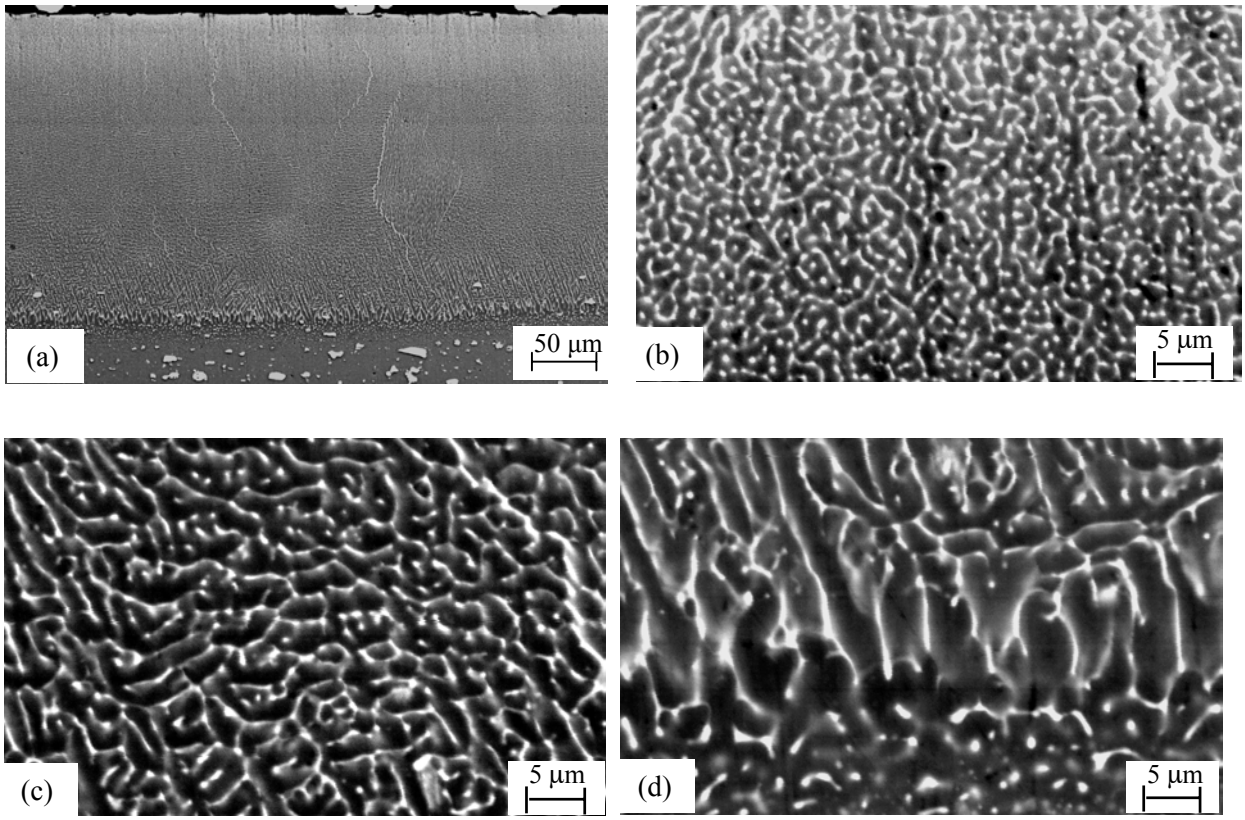

Figure 5 Scanning electron micrographs of the 6 mm line beam laser-melted 2014-T6 alloy, specimen A2; (a) overall view of the cross-sectional area (with melt depth 215 μm); (b) region close to the surface of the melt pool; (c) region in the middle of the melt pool (~ 100 μm away from the surface); (d) region close to the fusion boundary.

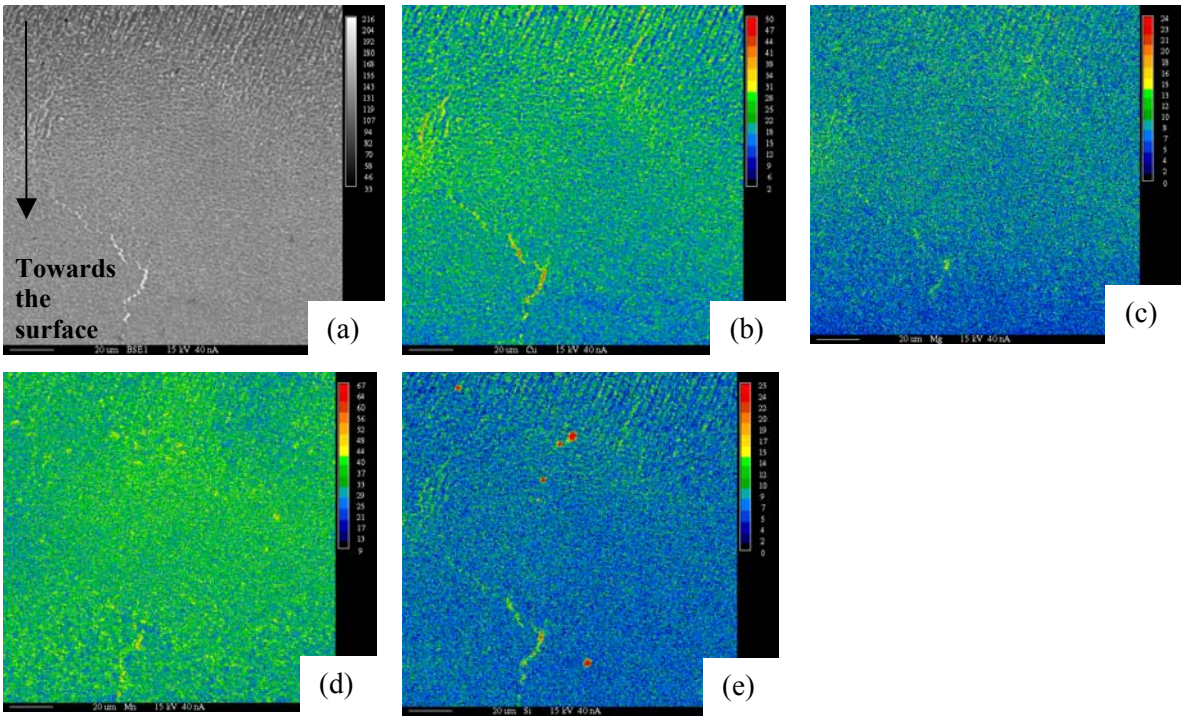

Figure 6 EPMA X-ray mapping of 6 mm laser-melted 2014-T451 alloy, specimen B1. (a) Backscatter image; (b) copper; (c) magnesium; (d) manganese; (e) silicon. (pictures are upside down)

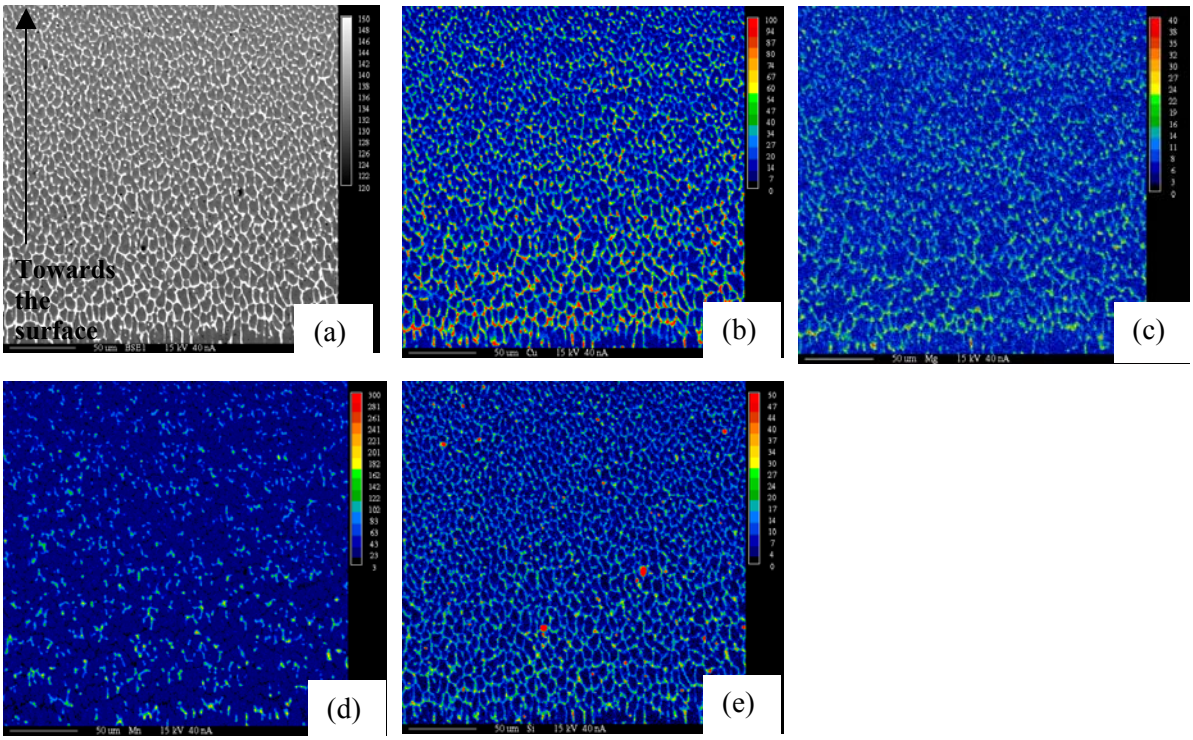

Figure 7 EPMA X-ray mapping of 10 mm laser–melted 2014-T451 alloy, specimen B5. (a) Backscatter image; (b) copper; (c) magnesium; (d) manganese; (e) silicon.

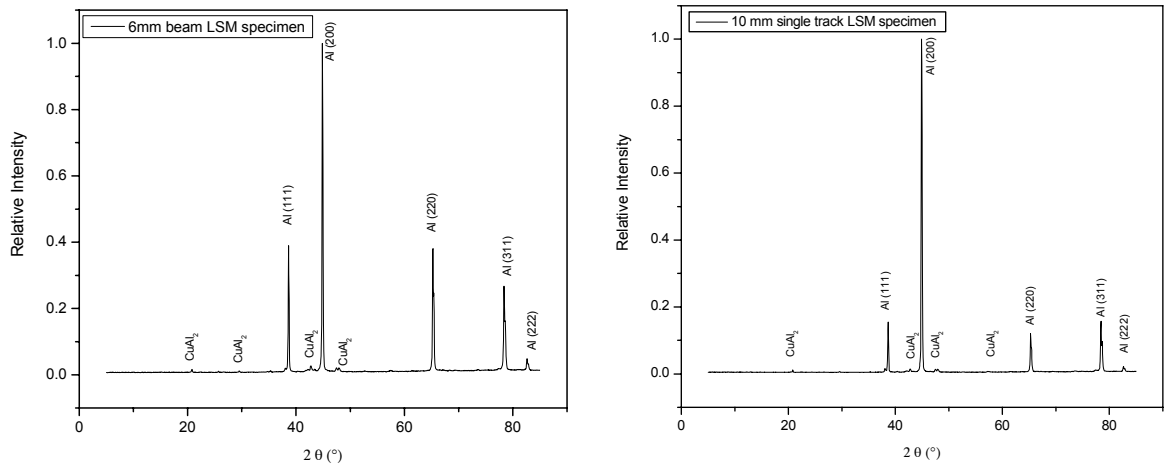

(a) (b)

Figure 8 XRD data of laser melted Al 2014-T6 alloy. (a) specimen A1; (b) specimen A5.

3.2 Pitting corrosion behaviour

The pitting potentials of the as-received Al 2014 alloy for the T6 and T451 tempers were -730 mV and –630 mV respectively (Table 2). A large number of pits, randomly distributed on the surface, were present after testing (Figure 9a). Although Al 2014 alloy in both tempers consisted of similar types of intermetallic particles, the copper content in the aluminium matrix for T6 is lower than that for T451. In the NaCl electrolyte, Al_2Cu, and Al-Cu-Mn-Fe-Si particles tend to be cathodic to the matrix [9], and pits are likely to initiate and grow in the copper-depleted zone around these particles [10]. Mg_2Si particles are anodic to the aluminium matrix, and have a tendency to dissolve and leaving cavities [11].

After laser treatment (Table 2), the pitting potentials decreased with the distance from the surface to the bottom of the melt pool. For instance, pitting potentials of B2 with grinding off of 20 μm and 100 μm were –515 mV and –560 mV respectively. Further, reduced pitting potentials were evident for the 6 mm beam. These trends correlate with coarsening of the dendritic structure and reducing of the copper concentration within the aluminium matrix with distance from the surface. The initial temper conditions did not influence pitting potentials of the laser-melted surfaces. However, with the T451 temper, improvement was only achieved using the 6 mm beam width,

possibly because of similarity of concentrations of alloying element in solid solution with the initial material and following treatment with the larger beam with slower cooling rate.

Pits formed on the laser-melted surfaces were larger but shallower than those in the as-received alloy, with a semi-continuous network, consisting of copper-rich precipitates, remaining within the pits, indicating their cathodic nature (Figure 9b). The size of the cells in the network was similar to the dendritic arm spacing found in non-corroded areas. Pitting apparently initiated in the cores of the dendrites, leading to dissolution of the matrix along the cell orientation and spreading to nearby areas.

Although significant reduction of the size of intermetallic particle after the laser melting was obtained for Al 2014-T451 treated by the 10 mm beam width, the pitting potential was not affected. Further, no improvement of pitting corrosion behaviour in laser-melted Al 2024-T351, Al 3003 and Al 7075 alloys occurs with rapidly solidified microstructures. Thus, the increase of pitting potentials after LSM cannot be attributed solely to the formation of a refined microstructure, with finer intermetallic particle, although such refinement might play an important role in metastable pitting process, such as by reduction of flaw densities in the passive film. Therefore, it is proposed the concentrations of solid solution alloy elements, particularly copper, are key factors influencing pitting corrosion. Such increase of copper content in the aluminium matrix can reduce the potential difference between the Al_2Cu phases and the aluminium matrix, thereby reducing the driving force for pitting corrosion. The reduction in population, or the elimination of Mg_2Si particles which are anodic to aluminium matrix may further improve the behaviour by reducing cavities due to the dissolved particles. Dissolution of such particles should increase with increased copper concentration in the matrix.

Regarding influences of preferred orientation, the literature [12] indicates that the pitting potential of aluminium increases in order of $(E_{pit})_{\{001\}} > (E_{pit})_{\{011\}} > (E_{pit})_{\{111\}}$, however, the presence of alloyed copper in solid solution reduces the dependence of E_{pit} on surface orientation. Thus, the preferred orientation of α-Al along [200]

direction in laser-treated alloy does not appear to play a significant role in the improved pitting behaviour.

Table 2 Pitting potential for Al 2014 alloy before and after LSM.

	distance from melted surface	Epit (mV)
As-received Al 2014-T6 alloy	-	-730
Laser melted (6 mm beam), specimen A1	100 μm	-560
Laser melted (10 mm beam), specimen A5	100 μm	-640
As-received Al 2014-T451 alloy	-	-623
Laser melted (6 mm beam), specimen B2	20 μm	-515
Laser melted (6 mm beam), specimen B2	100 μm	-560
Laser melted (10 mm beam), specimen B5	20 μm	-635
Laser melted (10 mm beam), specimen B5	140 μm	-620

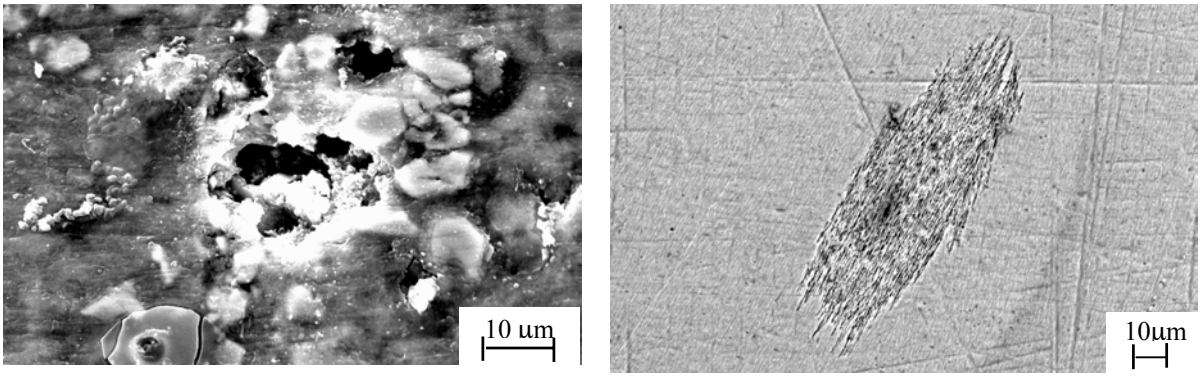

(a) (b)

Figure 9 Pit morphology of (a) as-received Al 2014-T6 alloy and (b) laser-melted Al 2014-T6 alloy.

4. Conclusion

1) LSM increased the pitting potential of Al 2014 alloy in the T6 and T451 tempers and changed the pitting morphology. The initial temper condition did not affect significantly the pitting corrosion behaviour of the laser-melted surfaces.
2) Conditions of more rapid cooling associated with increased retention of alloying elements, particularly copper, in solid solution and reduced microsegregration led to greatest improvement in pitting potentials. Thus, increased pitting potentials were achieved with faster scan rates, a smaller beam and with material closer to the surface of the melt pool.
3) The extensions of copper solubility in aluminium matrix was considered to be the key factor responsible for the increase of pitting potential, probably associated with the reduction of galvanic coupling between the Al_2Cu particles and the aluminium matrix.

Acknowledgements

The authors thank the Engineering and Physical Science Research Council (EPSRC) for financial support.

Reference:

1. E. McCafferty, P. G. Moore, Journal of the Electrochemical Society, 133, 6, pp1090-1096, 1986.
2. P. H. Chong, Z. Liu, P. Skeldon, G. E. Thompson, Applied Surface Science, 208-209, pp399-404, 2003.
3. R. Li, M. G. S. Ferreira, A. Almeida, R. Vilar, K. G. Watkins, M. A. McMahon, W. M. Steen, "Localized Corrosion of Laser Surface Melted 2024-T351 Aluminium Alloy", Surface and Coatings Technology, 81, pp290-296, 1996.
4. T. T. Wong and G. Y. Liang, Journal of Materials Processing Technology, 63, pp930-934, 1997.
5. E. McCafferty, P. G. Moore, G. T. Peace, Journal of the Electrochemical Society, 129 pp9-16, 1982.
6. M. A. McMahan, PhD Thesis, University of Liverpool, UK, 1994.
7. J. R. Davis, Aluminium and Aluminium Alloys, ASM Specially Handbook, pp.579-664.
8. Y. Liu, G.E. Thompson, P. Skeldon, C. J. E. Smith, K. Shimizu, "Chromate Conversion Coating Growth on Aluminum 2014-T6 Alloy", 2nd International Symposium on Aluminium Surface Science and Technology Proceedings (ASST 2000), pp479-484, 21-25 May 2000.
9. W. Kurz, R. Trivedi, Materials Science and Engineering A, 179-180, pp 46-55, 1994.
10. V. Guillaumin, G. Mankowski, "Localized Corrosion of 2024 T351 Aluminium Alloy in Chloride Media", Corrosion Science, Vol. 41(1999) 421-438.
11. Y. Liu, G. E. Thompson, P. Skeldon, C. J. E. Smith, K. Shimizu, Y. Kihn, "Inhibition of Corrosion of 2014-T6 by Chromate Species in a Chloride Environment", 2nd International Symposium on Aluminium Surface Science and Technology Proceedings (ASST 2000), pp473-478, 21-25 May 2000.
12. M. Yasuda, F. Weinberg and D. Tromans, Journal of the Electrochemical Society, 137, pp3708-3715, 1990.